INTERNATIONAL SOCIETY FOR
SOIL MECHANICS AND
GEOTECHNICAL ENGINEERING

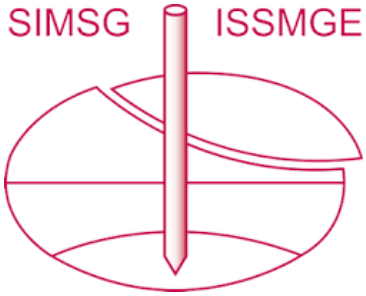

This paper was downloaded from the Online Library of the International Society for Soil Mechanics and Geotechnical Engineering (ISSMGE). The library is available here:

https://www.issmge.org/publications/online-library

This is an open-access database that archives thousands of papers published under the Auspices of the ISSMGE and maintained by the Innovation and Development Committee of ISSMGE.

The paper was published in the proceedings of the 11th International Conference on Scour and Erosion and was edited by Thor Ugelvig Petersen and Shinji Sassa. The conference was held in Copenhagen, Denmark from September 17th to September 21st 2023.

Internal soil erosion: A five-phase model and multi-physics SPH solver

Guodong. Ma,[1] Ha H. Bui,[2] Yanjian Lian[3], Giang D. Nguyen[4]

[1]Department of Civil Engineering, Monash University, Melbourne, Australia; e-mail: guodong.ma@monash.edu

[2]Department of Civil Engineering, Monash University, Melbourne, Australia; e-mail: ha.bui@monash.edu, Corresponding author.

[3]Department of Civil Engineering, Monash University, Melbourne, Australia; e-mail: yanjian.lian@monash.edu

[4]School of Civil, Environmental & Mining Engineering, University of Adelaide, Adelaide, Australia; e-mail: g.nguyen@adelaide.edu.au

ABSTRACT

This study presents a five-phase mathematical model capable of describing the seepage erosion-induced failures in earth structures. The five-phase model presented herein is formulated following the mixture theory, in which the multiphase mixture is assumed to be the superimpose of five homogenized phases (i.e., non-erodible coarse-particle phase, erodible fine-particle phase, fluidized-particle phase, water phase, and air phase). The advantage of the five-phase model is that it enables clear physical descriptions of the phase interactions (solid, fluid and air) and phase transformations (fluidization and deposition). A multi-physics smooth particle hydrodynamics (SPH) solver is subsequently adopted to solve this mathematical model, and results are compared with experimental data from the literature. The numerical results suggest that the proposed five-phase model, in combination with the multi-physics SPH solver, can reasonably describe the onset and post-failure of earth structures caused by seepage-induced internal erosion.

***Key Words*:** *Internal erosion, Multiphase model, SPH, Large deformation*

1. INTRODUCTION

Seepage-induced internal erosion significantly affects the integrity and stability of existing earth-retaining water structures such as dikes, levees, and dams. For example, nearly 46% of global embankment collapses were caused due to seepage-induced internal erosion (Foster et al. 2000). Other potential hazards, such as piping and sinkholes, also commonly happen due to internal erosion. Therefore, engineers need proper tools to foresee those events to prevent them from happening. Numerical modelling is such a tool that nowadays plays an essential role in predicting seepage

erosion and induced failures. However, current numerical models are only suitable for limited applications and hardly capture the entire onset and post-failure processes (Vardoulakis et al. 1996, Steeb et al. 2007, Yang et al. 2019, Lei et al. 2020). In this study, to overcome these drawbacks, a five-phase mathematical model describing the seepage erosion, a constitutive model reflecting the influence of erosion and the transient seepage flow, and a multi-physics SPH solver are presented. SPH is a mesh free method, and it shares the same library of the constitutive model with FEM. Because of these features, SPH has been widely used to solve challenging geotechnical problems (Bui and Nguyen 2017, Tran et al. 2019, Zhao et al. 2019, Wang et al. 2020, Yang et al. 2021). The proposed SPH computational model is applied to simulate an embankment collapse induced by seepage erosion, and numerical results are compared to the experiment. This paper is structured as follows: the numerical model is introduced in Section 2 after the Introduction section, and then the numerical prediction and results are shown in Section 3. Finally, the conclusions of the study will be presented in Section 4.

2. NUMERICAL MODEL

2.1 *A five-phase mathematical model for internal erosion*

Fig. 1(a) shows the physical erosion process in porous soil media. The soil is commonly unsaturated, consisting of three phases: air, water, and solid. When seepage-induced erosion happens, some fine erodible particles (a fraction of solid particles) can transform their state from solid to fluidized particles due to seepage forces. Reversely, some fluidized particles can deposit, becoming solid fines again. The fluidized particles exist in water and can be measured via concentration. Therefore, extra variables like fines content (fines fraction) and concentration are needed to describe the erosion process.
This study proposes a five-phase mathematical model to describe phase interactions (solid, fluid and air) and phase transformations (fluidization and deposition) during the internal erosion process. As shown in Fig. 1(b), the five-phase model includes soil skeleton (*ss*), erodible particles (*se*), water (*w*), fluidized particles (*sf*) and air phase (*a*). The soil skeleton and erodible particles together form the solid mixture (*s*), while fluidized particles and water form the fluid mixture (*f*). Each phase has their volume fraction $n_\alpha = V_\alpha / V_{RVE}$. Finally, the fines content is defined as $f_c = n_{se}/n_s$ and the concentration is defined as $C = n_{sf}/n_f$ to describe the erosion process.

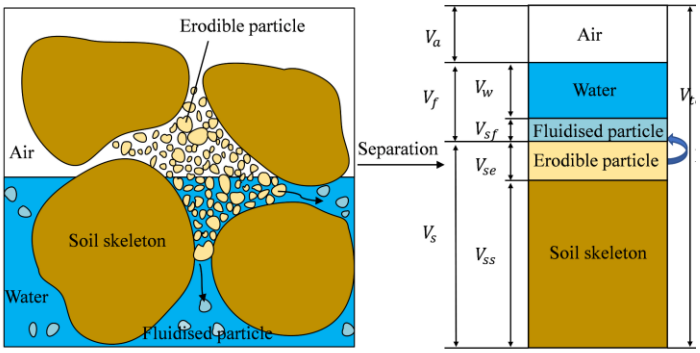

(a) (b)

Figure 1. Concept of a five-phase model

2.2 *Governing equations*

The governing equations of the entire five-phase mixture undergoing the internal erosion process can be established based on the continuum porous media theory. Table 1 summarises the key governing equations established through rigorous mathematical derivations (Ma et al. 2022). The porosity, fines content and concentration evolutions can be achieved using Equations (1) to (3), respectively. The momentum balance equation of the solid phase can be described using Eq.(4), considering the seepage interaction force. Darcy's law calculates the water or fluid velocity, assuming the water and fluid phase have the same velocity. Finally, the water/fluid pressure head is updated using Eq.(6), considering the fully coupled seepage erosion behaviour, like the influence of volumetric deformation and the density change due to erosion.

Table 1. Summary of governing equations

Variables	*Mathematical expressions*	*Eq. No.*
Porosity	$\frac{d\phi}{dt} = (1-\phi)\nabla \cdot \mathbf{v}_s + \hat{n}_s^{ex}$	(1)
Fines content	$\frac{df_c}{dt} = \frac{f_c - 1}{1-\phi}\hat{n}_s^{ex}$	(2)
Concentration	$\frac{dC}{dt} + (\mathbf{v}_f - \mathbf{v}_s)\nabla \cdot C = \hat{n}_s^{ex}(1 - C\frac{\rho_s}{\rho_f})/S_r\phi$	(3)
Momentum balance	$\bar{\rho}_s \frac{d\mathbf{v}_s}{dt} = \nabla \cdot \bar{\boldsymbol{\sigma}}_s + \bar{\rho}_s \mathbf{b} + \frac{\bar{\rho}_f \mathrm{g}}{k_f} n_f (\mathbf{v}_f - \mathbf{v}_s) - p_f \nabla n_f$	(4)
Darcy's law	$\boldsymbol{q}_f = \frac{k_f}{\rho_f \mathrm{g}}\left(-\nabla p_f + \rho_f \mathbf{b} - \rho_f \frac{d\mathbf{v}_s}{dt}\right)$	(5)
Pressure head	$\frac{dh}{dt} = \frac{1}{C_r}\left\{-S_r \nabla \cdot \mathbf{v}_s + \nabla \cdot \left[k_f\left(\nabla H + \frac{1}{\mathrm{g}}\frac{d^{ss}\mathbf{v}_s}{dt}\right)\right] + \left(\frac{\rho_s}{\rho_f} - S_r\right)\hat{n}_s^{ex}\right\}$	(6)

where ϕ is porosity; $\mathbf{v}_s$ and $\mathbf{v}_f$ are soil and fluid velocities; $\hat{n}_s^{ex}$ is volume exchange term due to erosion; f_c is fines content; C is concentration; p_f is pore fluid pressure; n_f is the volume fraction of fluid; $\bar{\rho}_s$ and $\bar{\rho}_f$ are the partial density of soil and fluid; $\bar{\boldsymbol{\sigma}}_s$ is the partial stress of the solid phase; $\boldsymbol{q}_f$ is fluid velocity vector; k_f is the hydraulic conductivity of fluid; ρ_f and ρ_s are fluid and soil density; $\mathbf{b}$ is body force vector; h is pore fluid pressure head; H is total fluid pressure head; g is gravity; C_r is storage coefficient $C_r = \left(\frac{S_r \phi \rho_f g}{K_f} + \frac{\phi d S_r}{dh}\right)$; S_r is the degree of saturation; K_f is the fluid bulk modulus.

In this study, the following volume exchange term (n_s^{ex}) considering both erosion and deposition is adopted:

$$\hat{n}_s^{ex} = \hat{n}_e + \hat{n}_d \tag{7}$$

where $\hat{n}_e$ is erosion rate whose form can be referred to (Cividini and Gioda 2004); $\hat{n}_d$ is deposition rates whose form can be referred to (Schaufler et al. 2013). They are described as following:

$$\hat{n}_e = \begin{cases} \lambda_e (f_c - f_{c\infty}) \left|\mathbf{q}_f\right| & (f_c > f_{c\infty}) \\ 0 & (f_c < f_{c\infty}) \end{cases} \tag{8}$$

$$\hat{n}_d = \lambda_d C \left|\mathbf{q}_f\right| \tag{9}$$

where λ_e and λ_d are constant parameters; $f_{c\infty}$ is ultimate fines content after erosion, which is assumed zero in this study.

2.3 *The fundamentals of SPH*

SPH is a fully mesh-free continuum method in which the computational domain is discretized using material points. These material points save information like mass, density, and velocity. The basic SPH equations approximating a function, the gradient and the Laplacian operator of a function have been given Eq.(10-12) in the literature (Monaghan 1992):

$$f(\mathbf{x}_i) = \sum_{j=1}^{N} \frac{m_j}{\rho_j} f(\mathbf{x}_j) W_{ij} \tag{10}$$

$$\nabla_i f(\mathbf{x}_i) = \sum_{j=1}^{N} \frac{m_j}{\rho_j} f(\mathbf{x}_j) \nabla_i W_{ij} \tag{11}$$

$$\nabla_i^2 f(\mathbf{x}_i) = 2 \sum_{j=1}^{N} \frac{m_j}{\rho_j} \left[f(\mathbf{x}_j) - f(\mathbf{x}_i)\right] \frac{\mathbf{x}_{ji} \cdot \nabla_i W_{ij}}{\left|\mathbf{x}_{ji}\right|^2} \tag{12}$$

where $\nabla_i f(\mathbf{x}_i)$ is the first-order gradient of function f; $\nabla_i^2 f(\mathbf{x}_i)$ is the Laplacian operator; the subscripts i and j refer to the quantity evaluated at the position of particle i and j, respectively; ρ_j and m_j are the density and mass of particle j, respectively; N is the total number of neighbouring particles located within the support domain of particle i; $\mathbf{x}_{ji}$ is the relative distance between two particles, defined by $\mathbf{x}_{ji} = \mathbf{x}_j - \mathbf{x}_i$; W_{ij} and

$\nabla_i W_{ij}$ are the kernel function and its first-order gradient, and h is the smoothing length defining the cut-off distance of the kernel function.

In this study, the cubic spline kernel function was adopted. Moreover, the authors adopted an improved SPH gradient and Laplacian operator Eqs. (13) and (14) for approximating general quantities because more accurate results can be achieved (Bui and Nguyen 2021):

$$\nabla_i^m f(\mathbf{x}_i) = \sum_{j=1}^{N} V_j \left[f(\mathbf{x}_j) - f(\mathbf{x}_i) \right] \widehat{\nabla}_i^m W_{ij} \tag{13}$$

$$\nabla_i^2 f(\mathbf{x}_i) = \frac{2}{K_{ij}} \left[\sum_{j=1}^{N} V_j f_{ji} \frac{\mathbf{x}_{ji} \cdot \nabla_i W_{ij}}{\left|\mathbf{x}_{ji}\right|^2} - \sum_{j=1}^{N} V_j f_{ji} \widehat{\nabla}_i^m W_{ij} \sum_{j=1}^{N} \frac{m_j}{\rho_j} \mathbf{x}_{ji}^m \frac{\mathbf{x}_{ji} \cdot \nabla_i W_{ij}}{\left|\mathbf{x}_{ji}\right|^2} \right] \tag{14}$$

where $\widehat{\nabla}_i^m W_{ij} = L_{ij}^{mn} \nabla_i^n W_{ij}$ and $L_{ij}^{mn} = \left[\sum_{j=1}^{N} \frac{m_j}{\rho_j} \left(x_j - x_i\right)^m \nabla_i^n W_{ij} \right]^{-1}$ is the renormalization matrix; $K_{ij} = \frac{1}{2} \left[\sum_{j=1}^{N} V_j \left(x_{ji}^2 + y_{ji}^2\right) \frac{\mathbf{x}_{ji} \cdot \nabla_i W_{ij}}{\left|\mathbf{x}_{ji}\right|^2} \right]$ and $f_{ji} = f(\mathbf{x}_j) - f(\mathbf{x}_i)$.

Recently, Lian et al.(Lian et al. 2021) further proposed a general SPH scheme for the approximation of second-order derivatives involving anisotropic diffusion, as shown in Eq. (15). They successfully applied this SPH scheme to solve rainfall-induced landslides with the anisotropic flow (Lian et al. 2022). It has been demonstrated that this SPH scheme can also be adopted in this study.

$$\frac{\partial^2 f_i}{\partial x^m \partial x^n} = \sum_{j=1}^{N} V_j \left(f_j - f_i\right) \mathcal{D}^{mn} \tilde{F}_{ij} - \frac{\partial f_i}{\partial x^{m'}} \sum_{j=1}^{N} V_j x_{ji}^{m'} \mathcal{D}^{mn} \tilde{F}_{ij} \tag{15}$$

where $\mathcal{D}^{mn} = 4 \frac{x_{ji}^m x_{ji}^n}{\left|x_{ji}\right|^2} - \delta^{mn}$ and $\tilde{F}_{ij} = \frac{\mathbf{x}_{ji}}{\left|x_{ji}\right|^2} \cdot \widehat{\nabla}_i W_{ij}$.

Furthermore, in order to complete the multi-physics SPH solver, a constitutive model suitable for seepage erosion has been developed based on the Drucker-Prager softening model (Ma et al. 2022). This model considers the influence of seepage flow on soil strength, specifically suction reduction, by formulating the evolution of suction and linking it to apparent cohesion. It also takes into account the influence of erosion on soil strength, i.e. mass loss, by linking the fines content to effective cohesion and friction angle. When seepage erosion occurs, the soil undergoes softening due to suction reduction and mass loss, resulting in a reduction of cohesion and friction angle. In the next section, we will present the results of numerical modelling conducted using this newly proposed five-phase model in combination with a multi-physics SPH solver.

3. NUMERICAL PREDICTIONS

3.1 *Seepage-induced internal erosion and embankment failure*

Bui and Nguyen (Bui and Nguyen 2017) presented an experimental study about erosion-induced embankment failure. Fig. 2 shows the geometry and setting conditions. A

constant 0.3 m water level was instantly applied to the upstream boundary, while 0 m water level was maintained at the downstream boundary. The soil properties are Young's modulus E 3.0 MPa, Poisson's ratio v 0.3, dry unit weight γ_s 25.5 kN/m^3, initial hydraulic conductivity k 1.1×10^{-4} m/s, initial porosity ϕ 0.4, and initial water content 5%. Fig. 3 shows the experimental observations of the embankment failure due to erosion. The whole failure process can be divided into two procedures. Firstly, local failure suddenly occurs at the slope toe as soil loses strength due to mass loss. Secondly, rotational failure and shear band develop, leading to the entire bank collapse.

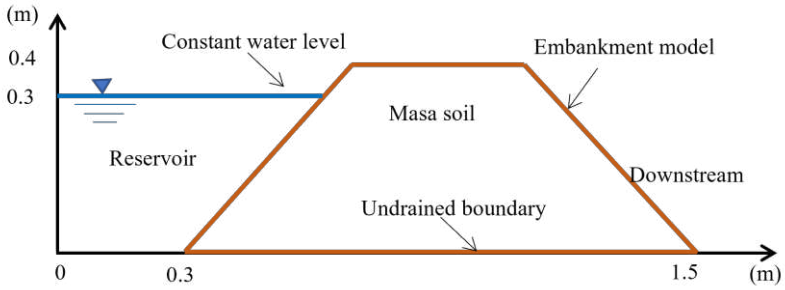

Figure 2. Geometry and setting conditions of an embankment (Bui and Nguyen 2017)

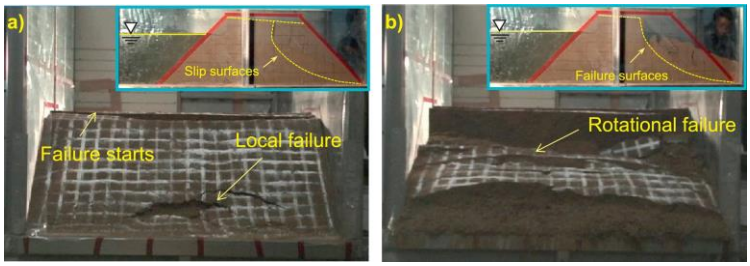

Figure 3. Experimental observation of the erosion-induced embankment failure (Bui and Nguyen 2017)

3.2 *Numerical results of the embankment failure*

The numerical modelling adopted the same geometry, boundary conditions and soil properties as mentioned in section 3.1 in this study. The initial fines content is reasonably chosen as 0.1 according to the grain size distribution of masa soil. The soil water retention curve used the Van-Genuchten model to describe the unsaturated seepage flow:

$$k_f = k_{sat}(\phi) S_e^{g_l} \left[1 - \left(1 - S_e^{\frac{g_n}{g_n - 1}} \right)^{\frac{g_n - 1}{g_n}} \right]^2 \quad (16)$$

where $S_e = (S_r - S_{res})/(S_{sat} - S_{res})$ is the effective saturation; s_{sat} and s_{res} are saturated and residual saturation degrees; g_n and g_l are constants that are chosen as 2.24

and 0, separately; $k_{sat}(\phi)$ is the saturated water hydraulic conductivity, which can be linked to the variation of porosity using the Kozeny-Carman equation.

The numerical results, such as the evolution of pore water pressure, fines content and plastic strain, are then plotted. Fig. 4 shows the evolution of pore water pressure. The negative pore water pressure (suction) gradually reduces during the transient seepage flow. After the steady state, the suction exists only above the phreatic line. These results show that our model can capture well the transient seepage flow process from unsaturated to saturated states, building a solid foundation for erosion analysis.

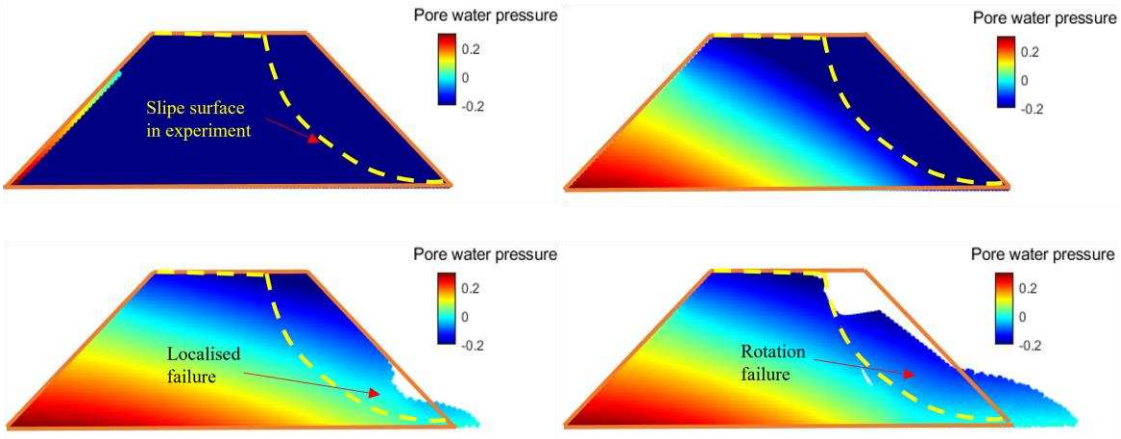

Figure 4. Evolution of pore water pressure

Fig.5 shows the evolution of the fines content. Firstly, the erosion process is triggered under the condition that the seepage velocity is larger than the critical seepage velocity when water reaches the downstream boundary. As erosion continues, the soil loses its mass and its shear strength, causing local failure. Finally, the shear band develops, and rotational failure can be observed in this numerical modelling.

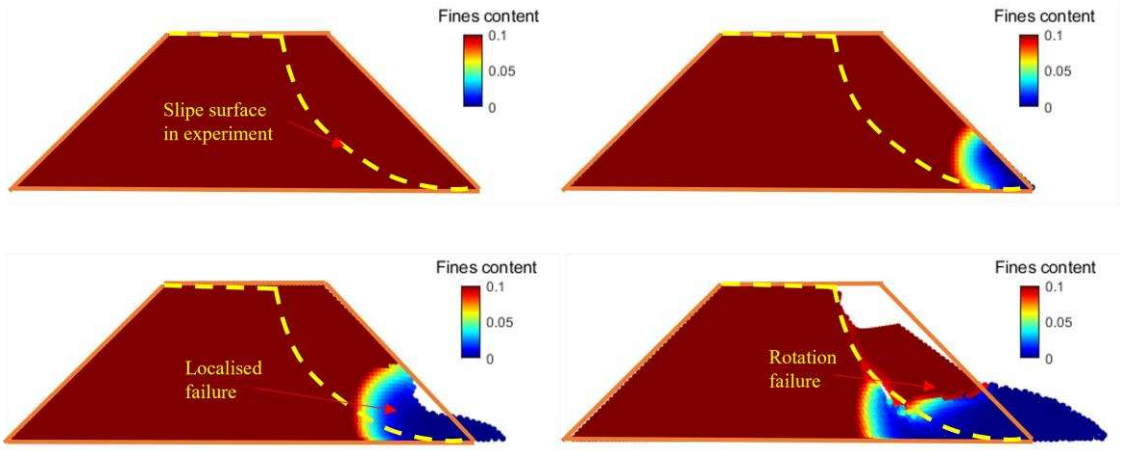

Figure 5. Evolution of fines content

Fig.6 shows the deformation process by capturing the evolution of the accumulated deviatoric plastic strain. After the soil loses its shear strength due to mass loss, the embankment becomes unstable at the toe area, causing local failure. Subsequently, the rotational failure occurs, and the shear band forms. These numerical results are consistent with the experimental observation, which demonstrated that our numerical model could simulate the boundary value problem involving seepage erosion and induced failure. Furthermore, compared to the experimental study, it can capture typical features such as local and rotational failures due to seepage erosion.

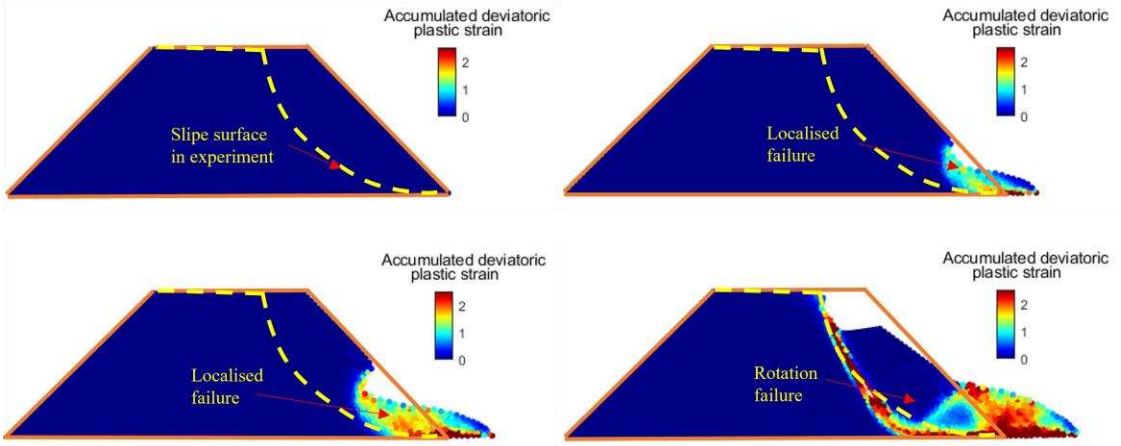

Figure 6. Evolution of accumulated deviatoric plastic strain

4. CONCLUSIONS

This study presented the application of a five-phase mathematical erosion model and multi-physics SPH solver to simulate seepage-induced internal erosion and failure of an earth structure. The paper demonstrated that the proposed SPH computational model has the advantage of predicting the transient seepage flow, localized failure at the slope toe caused by internal erosion, and the subsequent rotational progressive embankment failure. In future, this model can be used to predict other engineering problems like sinkholes, embankment piping, levee failure and so on due to seepage erosion.

5. ACKNOWLEDGMENTS

The authors gratefully acknowledge the financial support from the Australian Research Council via Discovery Projects DP190102779 (Bui & Nguyen) and FT200100884 (Bui). Part of this research was undertaken with the assistance of resources and services from the National Computational Infrastructure (NCI), supported by the

Australian Government. The author also gratefully thanks the support of the China Scholarship Council (CSC).

REFERENCE

Bui, H. H. and G. D. Nguyen (2017). "A coupled fluid-solid SPH approach to modelling flow through deformable porous media." International Journal of Solids and Structures 125: 244-264.
Bui, H. H. and G. D. Nguyen (2021). "Smoothed particle hydrodynamics (SPH) and its applications in geomechanics: From solid fracture to granular behaviour and multiphase flows in porous media." Computers and Geotechnics 138: 104315.
Cividini, A. and G. Gioda (2004). "Finite-element approach to the erosion and transport of fine particles in granular soils." International Journal of Geomechanics 4(3): 191-198.
Foster, M., R. Fell and M. Spannagle (2000). "The statistics of embankment dam failures and accidents." Canadian Geotechnical Journal 37(5): 1000-1024.
Lei, X., S. He, X. Chen, H. Wong, L. Wu and E. Liu (2020). "A generalized interpolation material point method for modelling coupled seepage-erosion-deformation process within unsaturated soils." Advances in Water Resources: 103578.
Lian, Y., H. H. Bui, G. D. Nguyen, H. T. Tran and A. Haque (2021). "A general SPH framework for transient seepage flows through unsaturated porous media considering anisotropic diffusion." Computer Methods in Applied Mechanics and Engineering 387: 114169.
Lian, Y., H. H. Bui, G. D. Nguyen, S. Zhao and A. Haque (2022). "A computationally efficient SPH framework for unsaturated soils and its application to predicting the entire rainfall-induced slope failure process." Géotechnique: 1-19.
Ma, G., H. H. Bui, Y. Lian, K. M. Tran and G. D. Nguyen (2022). "A five-phase approach, SPH framework and applications for predictions of seepage-induced internal erosion and failure in unsaturated/saturated porous media." Computer Methods in Applied Mechanics and Engineering 401: 115614.
Monaghan, J. J. (1992). "Smoothed particle hydrodynamics." Annual review of astronomy and astrophysics 30(1): 543-574.
Schaufler, A., C. Becker and H. Steeb (2013). "Infiltration processes in cohesionless soils." ZAMM-Journal of Applied Mathematics and Mechanics/Zeitschrift für Angewandte Mathematik und Mechanik 93(2-3): 138-146.
Steeb, H., S. Diebels and I. Vardoulakis (2007). Modeling internal erosion in porous media. Computer Applications In Geotechnical Engineering: 1-10.
Tran, H. T., Y. Wang, G. D. Nguyen, J. Kodikara, M. Sanchez and H. H. Bui (2019). "Modelling 3D desiccation cracking in clayey soils using a size-dependent SPH computational approach." Computers and Geotechnics 116: 103209.
Vardoulakis, I., M. Stavropoulou and P. Papanastasiou (1996). "Hydro-mechanical aspects of the sand production problem." Transport in porous media 22(2): 225-244.
Wang, Y., H. T. Tran, G. D. Nguyen, P. G. Ranjith and H. H. Bui (2020). "Simulation of mixed-mode fracture using SPH particles with an embedded fracture process zone." International Journal for Numerical and Analytical Methods in Geomechanics 44(10): 1417-1445.
Yang, E., H. H. Bui, G. D. Nguyen, C. E. Choi, C. W. W. Ng, H. De Sterck and A. Bouazza (2021). "Numerical investigation of the mechanism of granular flow impact on rigid control structures." Acta Geotechnica 16(8): 2505-2527.

Yang, J., Z. Y. Yin, F. Laouafa and P. Y. Hicher (2019). "Internal erosion in dike-on-foundation modeled by a coupled hydromechanical approach." International Journal for Numerical and Analytical Methods in Geomechanics 43(3): 663-683.
Zhao, S., H. H. Bui, V. Lemiale, G. D. Nguyen and F. Darve (2019). "A generic approach to modelling flexible confined boundary conditions in SPH and its application." International Journal for Numerical and Analytical Methods in Geomechanics 43(5): 1005-1031.